https://doi.org/10.1016/j.tsf.2021.138741

Strain-induced band gap tuning in flexible ferroelectric/mica thin films

Yu Sun[1,2], Ki Hei Wong[2], Kin Wing Kwok[2,*]

[1] Academy of Advanced Interdisciplinary Research, School of Advanced Materials and Nanotechnology, Xidian University, Xi'an 710126, China

[2] Department of Applied Physics, The Hong Kong Polytechnic University, Kowloon, Hong Kong, China

[*]Corresponding authors: apkwkwok@polyu.edu.hk

Abstract

Precise control of the band gap is crucial for lead-free ferroelectrics in the application of high-performance optical devices. In this work, we demonstrate that continuous and reversible tuning of optical band gap can be realized through mechanical strain in flexible $Ba_{0.9}Ca_{0.1}Ti_{0.975}Fe_{0.025}O_3$ (BCTF)/mica films. Through bending the flexible films, a large mechanical strain of 0.85% could be introduced into the ferroelectric active layer, leading to a reduction in the band gap of 0.38 eV. The strong dependence of the optical band gap on mechanical bending mainly arisen from the strain-induced modification of Fe-O bond. Because of the superior mechanical property of mica, the flexible BCTF/mica film also exhibits excellent anti-fatigue characteristics over 10^3 bending cycles. Thus, this work provides an alternate perspective for the design and fabrication of ferroelectric optical devices that cover the entire visible light region.

Key words: ferroelectric; thin film; strain; band gap

1. Introduction

ABO_3-type perovskite ferroelectric (FE) oxides show great potential in the field of energy conversion, such as photovoltaic cell, solar water splitting.[1-5] However, the energy conversion efficiency is generally restricted by their large band gaps ($E_g \approx$ 3-4 eV) which limits the solar energy harvesting to a small part of the spectrum.[6, 7] It is mainly resulted from the large difference of electronegativity between the B-site transition metal cations and oxygen.[8] Prior works have focused on chemical substitution as a means for reducing their gaps, but with unintended consequences for other properties.[9] Since the optical absorption of FE oxides is related to the electron transition from the occupied O 2*p* orbitals (the top of the valence band) to unfilled B-site cation *d* orbitals (the bottom of the conduction band), modifying the B−O bond properties can effectively tailor the band gap.[10, 11] Strain engineering has provided another route to tune the electronic structure through epitaxial mismatch strain.[12] However, owing to the small lattice mismatch and then tensile strain, only a small reduction (0.09 eV) in the band gap is realized. Similar results have been found in our previous work that a lattice expansion can delocalize electrons from B-site cations and induce a small reduction (0.1 eV) in the band gap for non-FE $LaFeO_{3-x}$ films.[13] In addition, the epitaxial strain can also change the local crystal field of the BO_6 octahedral. And the enhanced d-d transition forms a narrower sub-band gap in FE $YFeO_3$ films, resulting in a reduction in the band gap of 0.16 eV.[14] Although great research progresses have been achieved in tuning the band gap of FE oxides through mechanical strain,[15] developing approaches of tailoring their band gap in large scale with a continuous and reversible manner will bring significant scientific and technological breakthroughs in FE devices.

Inspired by the recent breakthroughs in the fabrication of inorganic oxide films on flexible mica substrate,[15-19] we have developed an effective approach to manipulate the band structure of FE oxides in a continuous and reversible manner by mechanical strain through substrate bending. It is realized with flexible ferroelectric $Ba_{0.9}Ca_{0.1}Ti_{0.975}Fe_{0.025}O_3$ (BCTF) epitaxial thin films fabricated on mica substrates. The effects of mechanical strain on the band gap have been investigated through UV-Vis absorption spectrum. In-situ Raman analysis has been used to examine the changes in lattice structure induced by the mechanical strain. The stability of the flexible film structures has been evaluated via continuous bending. Our results have demonstrated that the mechanical strain can change the structure of BO_6 octahedral and induce a large red-shift of 110 nm in optical

absorption, or a reduction of 0.38 eV in the band gap. The inter-relationships between the strain, structure and optical properties have been elucidated for providing a rational design strategy for flexible optical FE devices.

2. Experimental Section

2.1 Fabrication of BCTF target

$Ba_{0.9}Ca_{0.1}Ti_{0.975}Fe_{0.025}O_3$ (abbreviated as BCTF) FE ceramics were prepared by a conventional solid-state method using high-purity metal oxides or carbonate powders: $BaCO_3$ (99.5%), $CaCO_3$ (99%) TiO_2 (99.9%) and Fe_2O_3 (99.0%). The ceramic fabrication processes can be found in our previous work.[20] The ceramics were finally sintered in air at 1400°C for 4 hours. After confirming the crystallite structure and purity using X-ray diffraction (XRD) analysis, the ceramics were used as targets for preparing epitaxial thin films using the pulsed laser deposition technique.

2.2 Epitaxial growth of flexible BCTF/Mica films

(00*l*)-cut fluorophlogopite mica ($KMg_3(AlSi_3O_{10})F_2$ (Changchun Taiyuan Co., Ltd., China) were used as substrates (of dimensions 10 cm ×10 cm) in this work. 100 nm BCTF film was directly deposited on mica using the pulsed laser deposition technique. The target was ablated at 750°C (substrate temperature) with a target-to-substrate distance of 48 mm in pure oxygen of 15 Pa by a KrF excimer laser (λ = 248 nm) operated at 6 Hz with an energy density of 1.5 J/cm^2. After 25 min deposition, the film was post-annealed in situ at 750°C in an oxygen pressure of 10^4 Pa for 30 min to reduce oxygen vacancies. The as-grown sample was cooled down to room temperature at a rate of 5 °C/min. To acquire good mechanical flexibility for the bending experiment, the two-dimensional layered mica substrate was mechanically exfoliated to a thickness of 30 μm using tape. Another sample with a conductive LSMO film bottom electrode inserted between BCTF film and mica substrate was used for ferroelectricity analysis. Au top electrode of area 1 mm^2 was finally deposited on the film surface using E-beam evaporation for the electrical measurements. The thickness of the LSMO bottom electrode, BCTF film and Au top electrode are 50 nm, 100 nm and 20 nm, respectively.

2.3 Thin film characterization

The crystal structure and epitaxial nature of the BCTF/mica film were examined using high-resolution XRD (SmartLab, Rigaku Co.) equipped with Cu $K_{\alpha1}$ (λ =

1.5406 Å). The surface morphology was examined using Atomic Force Microscopy (AFM, Asylum MFP-3D Infinity, Oxford). The transmittance spectra were recorded using a UV-Vis spectrometer (Shimadzu Co. UV 2550). The Raman spectra were recorded using a confocal Raman system (WITec alpha300 R). The ferroelectricity of the BCTF films was evaluated based on their polarization hysteresis (P-E) loops measured at room temperature (Precision Premier II, Radiant Technologies Inc.). And a triangular wave electrical signal with a frequency of 1000 Hz was applied to the FE films.

2.4 Strain engineering

In order to facilitate the transmission of light for UV-Vis test, we opened a rectangular gap (8 × 2 mm) in the stainless steel by laser cutting. Then, the controllable mechanical strains in the BCTF thin films were introduced by taping the flexible BCTF/mica samples on stainless steel holder with various radii of curvature. And the radii of curvature were controlled by changing the distance between the two sides of stainless steel holder.

3. Results and Discussion:

The XRD patterns of the BCTF/mica films are shown in Fig. 1a. The BCTF film possesses a typical P-4mm space group, which is similar to the structure of tetragonal $BaTiO_3$ ferroelectrics. As demonstrated by the appearance of only (111) and (222) reflections, the BCTF film has a single-phase structure and preferentially grown along the [*l l l*] direction. The epitaxial relationship between the BCTF film and mica substrate is investigated based on their XRD ϕ scans measured on their (101) and (202) reflection peaks, respectively (Fig. 1b). Ascribed to the trifold symmetry of mica, the BCTF film exhibits six-fold symmetric reflection peaks at 60° intervals. This clearly suggests the good epitaxial feature of the BCTF film on the mica substrate. As revealed by the surface morphology image shown in Fig. 1c, the BCTF/mica film exhibits a flat surface with a root mean square roughness of 2.49 nm, which also indicates a uniform thickness of 105.4 nm (Fig. 1d,e). Tetragonal crystals (such as $BaTiO_3$) normally adopt a tri-fold symmetry along [111] orientation. The six-fold symmetry observed in the BCTF (*lll*) film may be resulted from the 180^o twin domains.[20] The out-plane and in-plane epitaxial relationships can be described as (111)BCTF || (001)Mica and [1 -1 0]BCTF || [010]Mica. We then obtained the in-plane lattice arrangement for the BCTF unit cell on a mica substrate as shown in Fig. 1d. Because the lattice parameter of

BCTF along [1 -1 0] is slight larger than 1/2 b_{Mica}, the epitaxial BCTF film shows a compression stress in-plane.

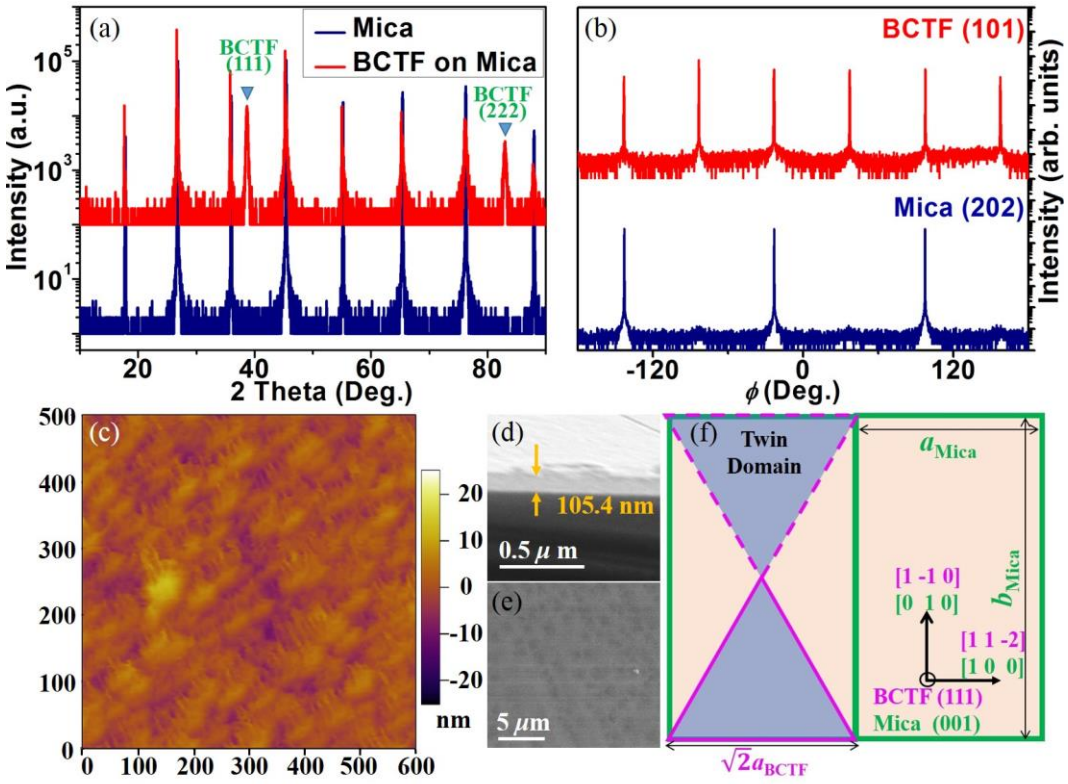

Figure 1. (a) XRD θ-2θ scan spectra of bare mica, BCTF on mica (0 0 *l*) substrates; (b) XRD ϕ scans of the BCTF (101) and mica (202) reflection peaks, (c) AFM image for the surface morphology analysis of BCTF film, SEM images for BCTF/Mica film cross section (d) and in plane (e), (f) Schematic of in-plane lattice arrangement for BCTF unit cell on the monoclinic mica substrate.

It has been known that the doping of transition metal cations with non-d^0 configuration at the B site of perovskite-type FE oxides can form a new sub-band gap.[9] The effect of Fe-doping on the as-grown BCTF/mica films has then been investigated. As shown in Fig. 2a, the mica substrate exhibits a high transmittance (over 85 %) in the visible region together with a strong absorption at wavelengths shorter than 370 nm. Attributed to the BCTF layer, the as-grown BCTF/mica film exhibits two absorption peaks. The strong absorption around 370-400 nm should be attributed to the Ti^{4+} which matches well with the band gap of $BaTiO_3$ (~3.2 eV)[21], whereas the absorption around 500-550 nm should be resulted from the Fe^{3+} dopant which agrees with the band gap (~2.4 eV) observed in Fe-based perovskite oxides.[13]

For studying the mechanical strain effect on the optical band gap, the BCTF/mica films have been bent to different extents using a simple device shown in the insert of Fig. 2a. Via precisely controlling the distance (l) between the two sides of the film (Fig. 2b), a quasi-circular arc with different radii of curvature (r) (corresponding to center angle of θ radian) is formed and then a tensile strain (ε) can be exerted on the BCTF film. In this work, mica owns a size of a = 10.0 mm and thickness h = 0.03 mm. Combining with the following relationship,

$$l = 2 \text{ Sin } (\theta/2)$$
$$a = r \cdot \theta$$

we could obtain the tensile strain value $\varepsilon = [(h + r)\theta - r\theta] / r\theta = h / r$ (Fig. 2b). So, we could apply the maximum strain to the film when $a = \pi r$, namely ε_{max} = 0.94%. Because of the superior mechanical property of mica, the strained flexible BCTF/mica film belongs to elastic deformation. In this work, a large tensile strain of ~ 0.85 % is realized at l = 7.0 mm. The UV-Vis transmittance spectra of the BCTF/mica film in different bent states (with different l) have then been measured, giving the results shown in Fig. 2c. Both the absorption peaks attributed to Ti^{4+} and Fe^{3+} exhibit a clear shift to longer wavelengths (i.e., red shift). For the Fe-peak, the absorption cutoff shifts from 550 nm to 660 nm (as denoted by a dotted line in Fig. 2c), suggesting that the tensile strain can effectively tune the band gap of FE oxides. To provide evidence, the optical band gap E_g of the films is estimated from the Tauc plots. Accordingly, the absorption coefficient α is calculated from the transmittance T by

$$\alpha = 1/t \text{ Log } (1/T\%)$$

where t is the thickness of the BCTF film (100 nm). With the assumption of direct transition, the relationship between E_g and α is given as:

$$(\alpha h\nu)^2 = A\ (h\nu - E_g)$$

where ν is the photon frequency, h is Planck's constant and A is a constant.

Due to the larger electronegativity of Fe^{3+} than that of Ti^{4+}, it will introduce a new electronic state of Fe 3d with lower energy in the original band gap.[22, 23] As shown in Fig. 2d, all the films (in different states) exhibit a weak absorption peak around 2.5 eV, which is attributed to the Fe^{3+} dopant. By extrapolating the linear portion of the curve to zero (as denoted by the dotted lines in Fig. 2d), the E_g for the films in different strain states are determined. For perovskite oxides, the top of the valence band are mainly occupied by the filled 2p orbits of oxygen, while the

bottom of the conduction band (CB) are formed by the empty *d* orbits of B-site transition metal cations.[24] Here, the mechanical strain modifies the B-O bonds, and thus inducing a slight change in the crystal field of BO_6 and then a decrease in the hybridization between O 2*p* and Fe 3*d* orbits.[25] Consequently, a drop in energy of the hybridized 3*d* orbits will narrow the gap between CB and VB, and then lead to a smaller optical band gap.[26, 27]

As shown in Fig. 2e, the observed E_g shows a strong dependence on the mechanical strain. It remains almost unchanged at ε below 0.4%, and then decreases rapidly from 2.27 eV to 1.89 eV as ε increases to 0.85%. These suggest that the E_g can be effectively adjusted within the visible region through mechanical strain. It should be noted that the flexible BCTF/mica film could afford a larger mechanical strain. But a larger strain means a smaller radius of curvature. The stainless-steel holders will not permit the UV transmission test.

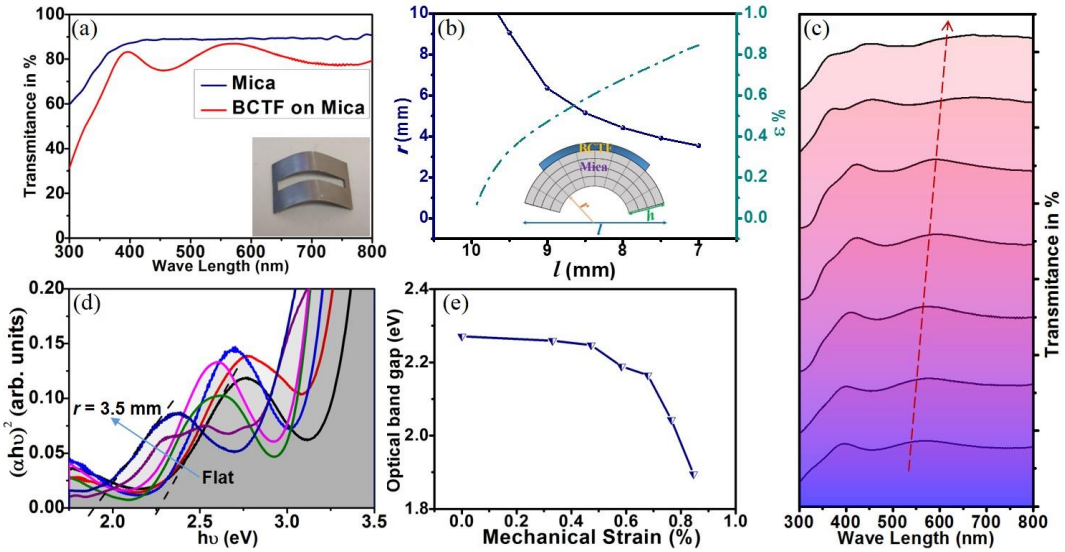

Figure 2. (a) UV-Vis transmittance spectra for bare mica and BCTF/mica film, the insert shows the simple device for bending test; (b) The relationship between the distance (*l*) for two sides of mica substrate and theoretical mechanical strain, the insert shows the diagram for mechanical strain; (c) The dependency of transmittance spectra on different mechanical strain; (d) The Tauc plots calculated based on Kubelka–Munk functions to show the optical band gaps with different mechanical strain; (e) The effect of mechanical strain on the optical band gap for BCTF films.

Owing to the high sensitivity to local ionic configurations, in-situ Raman spectroscopy has been used to investigate the crystal structure evolution during the bending process. As shown in Fig. 3a, the spectrum for the film in the flat state exhibits a weak peak at 308 cm^{-1}, which is related to the [B_1] vibration and considered as a salient feature for distinguishing the ferroelectric tetragonal phase from the paraelectric cubic phase.[28] The shoulder remains at different bent states, but is overlaid by a Raman band attributed to the [A_1(TO)] vibration or the stretching of B-O bonds (Fig. 3b).[29] After Lorentzian fitting for these Raman peaks, the band locates at 225 cm^{-1} for the film in the flat state exhibits a blue shift to 263 cm^{-1} as the strain increases to 0.85 % (l = 7.0 mm). As the vibration is related to the stretching of the B-O bond of the BO_6 octahedral, the observed blue shift provides evidence of the elongated B-O bond which induces a reduction in bang gap as discussed.[30, 31] As also shown in Fig. 3a, the Raman band attributed to the [A_1(TO4)] vibrations (Fig. 3c) shifts slightly from 517 cm^{-1} to 502 cm^{-1} as the mechanical strain increases from 0 to 0.85 %. This indicates that the B-site cations are moved from the symmetric center, and thus increasing the asymmetry of the BCTF crystal structure, which should then be favorable for retaining the intrinsic ferroelectricity.[32-34] It can be induced from the loops that the quality of the loop only starts to improve and to show some ferroectric activity in the film under strength. Compared with the original BCTF, the ferroelectric polarization for films with 0.85% mechanical strain increases faster at the same electric field (Fig. 3d).

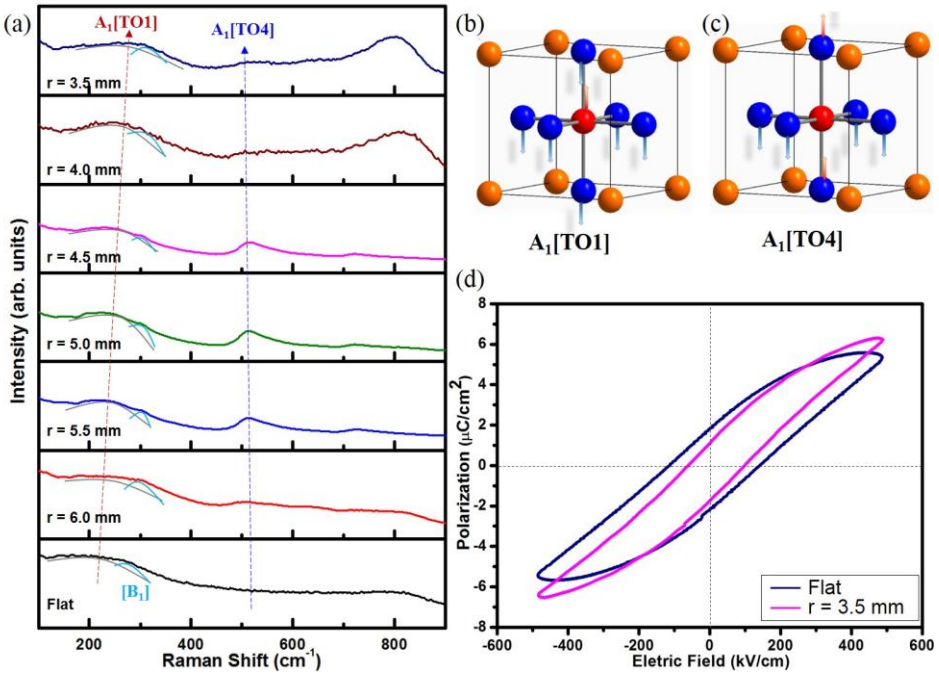

Figure 3. (a) The Raman spectra for BCTF films with different ROCs; Diagram for different Raman vibrations in BCTF (b) [A_1(TO)] and (c) [A_1(TO4)]; (d) PE loop with maximum and minimum strain.

Optical devices with stable performances are generally required for practical applications. For evaluating the reversibility as well as stability of the induced change in the band gap, the UV-Vis transmittance spectrum of the flexible BCTF/mica film subjected to cyclic bending (up to 10^3 cycles) have been investigated, giving the results shown in Fig. 4a. It can be seen that the spectra of film in both the flat (l = 10 mm) and bent (l = 7.0 mm) states remain almost unchanged after 10^3 cycles of bending. Similarly, the calculated band gap of the film in the flat and bent states remain almost the same after different cycles of bending (Fig. 4b), i.e., retaining at about 2.27 ± 0.01 eV in the flat state (l = 10.0 mm) and 1.89 ± 0.02 eV in the bent state (l = 7.0 mm). These clearly demonstrate the good reversibility and high stability of the structural change and band gap induced by the mechanical strain.

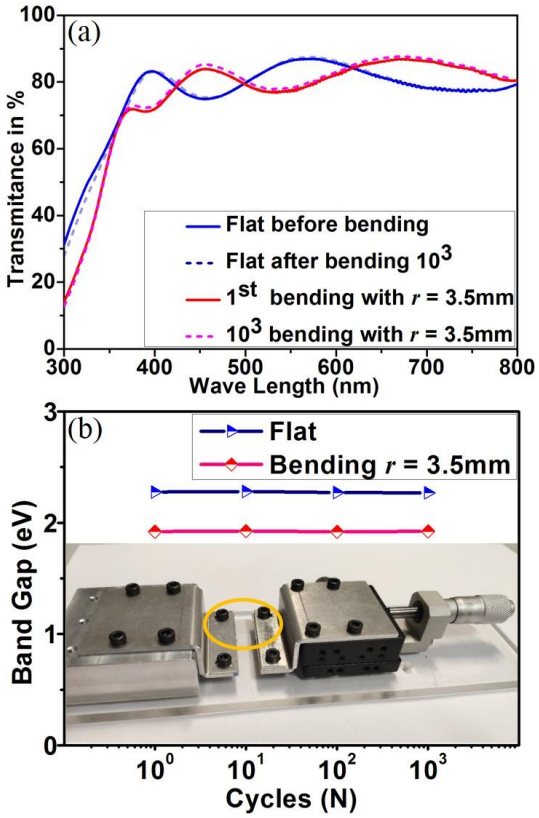

Figure 4. Stability characterization in both the flat and bending states: (a) The UV-Vis transmittance spectra for BCTF/mica films before and after bending 10^3 cycles; (b) The band gap for several interval cycles during cycling test.

4. Conclusion

In summary, we report a continuous and reversible method to tailor the optical band gap of $Ba_{0.9}Ca_{0.1}Ti_{0.975}Fe_{0.025}O_3$/mica epitaxial thin film through mechanical strain. The non-decay response in UV-Vis transmittance spectra indicates a strong dependency of optical band gap on the mechanical strain. Raman spectra reveal that the large red shift in absorption cutoff results from the strain-induced modification of B-O bond. Based on the excellent mechanical flexibility for mica substrates, the BCTF/mica FE films exhibit superior stability for mechanical bending over 10^3 cycles. Thus, our results offer a general strategy to reversibly manipulate the band structure for ferroelectric oxides. It will open up a leap for the design and fabrication of optical devices with giant potential in the field of energy conversion, photodetector, information storage.

Declaration of Competing Interest

The authors declare that they have no known competing financial interests or personal relationships that could have appeared to influence the work reported in this paper.

Acknowledgements

This work was supported by the National Natural Science Foundation of China (21801089), Research Grants Council of the Hong Kong Special Administrative Region (PolyU 152236/17E), The Hong Kong Polytechnic University (1-ZVGH), the Fundamental Research Funds for the Central Universities.

References

[1] M. Yang, D.J. Kim, M. Alexe, Flexo-photovoltaic effect, Science, 360 (2018) 904-907.
[2] S.Y. Yang, J. Seidel, S.J. Byrnes, P. Shafer, C.H. Yang, M.D. Rossell, P. Yu, Y.H. Chu, J.F. Scott, J.W. Ager, 3r
d, L.W. Martin, R. Ramesh, Above-bandgap voltages from ferroelectric photovoltaic devices, Nature nanotechnology, 5 (2010) 143-147.
[3] L.W. Martin, A.M. Rappe, Thin-film ferroelectric materials and their applications, Nature Reviews Materials, 2 (2016).
[4] J. Song, T.L. Kim, J. Lee, S.Y. Cho, J. Cha, S.Y. Jeong, H. An, W.S. Kim, Y.-S. Jung, J. Park, G.Y. Jung, D.-Y. Kim, J.Y. Jo, S.D. Bu, H.W. Jang, S. Lee, Domain-

engineered $BiFeO_3$ thin-film photoanodes for highly enhanced ferroelectric solar water splitting, Nano Research, 11 (2017) 642-655.
[5] J. Xie, C. Guo, P. Yang, X. Wang, D. Liu, C.M. Li, Bi-functional ferroelectric BiFeO3 passivated $BiVO_4$ photoanode for efficient and stable solar water oxidation, Nano Energy, 31 (2017) 28-36.
[6] I. Grinberg, D.V. West, M. Torres, G. Gou, D.M. Stein, L. Wu, G. Chen, E.M. Gallo, A.R. Akbashev, P.K. Davies, J.E. Spanier, A.M. Rappe, Perovskite oxides for visible-light-absorbing ferroelectric and photovoltaic materials, Nature, 503 (2013) 509-512.
[7] R. Guo, L. You, Y. Zhou, Z.S. Lim, X. Zou, L. Chen, R. Ramesh, J. Wang, Non-volatile memory based on the ferroelectric photovoltaic effect, Nature communications, 4 (2013) 1990.
[8] P. Machado, M. Scigaj, J. Gazquez, E. Rueda, A. Sanchez-Diaz, I. Fina, M. Gibert-Roca, T. Puig, X. Obradors, M. Campoy-Quiles, M. Coll, Band Gap Tuning of Solution-Processed Ferroelectric Perovskite $BiFe_{1-x}Co_xO_3$ Thin Films, Chemistry of materials : a publication of the American Chemical Society, 31 (2019) 947-954.
[9] S. Das, S. Ghara, P. Mahadevan, A. Sundaresan, J. Gopalakrishnan, D.D. Sarma, Designing a Lower Band Gap Bulk Ferroelectric Material with a Sizable Polarization at Room Temperature, ACS Energy Letters, 3 (2018) 1176-1182.
[10] R. Nechache, C. Harnagea, S. Li, L. Cardenas, W. Huang, J. Chakrabartty, F. Rosei, Bandgap tuning of multiferroic oxide solar cells, Nature Photonics, 9 (2014) 61-67.
[11] F. Wang, I. Grinberg, A.M. Rappe, Band gap engineering strategy via polarization rotation in perovskite ferroelectrics, Applied Physics Letters, 104 (2014) 152903.
[12] H. Wang, F. Khatkhatay, J. Jian, J. Huang, M. Fan, H. Wang, Strain tuning of ferroelectric and optical properties of rhombohedral-like $BiFeO_3$ thin films on SrRuO3-buffered substrates, Materials Research Bulletin, 110 (2019) 120-125.
[13] Y. Sun, X. Wu, L. Yuan, M. Wang, M. Han, L. Luo, B. Zheng, K. Huang, S. Feng, Insight into the enhanced photoelectrocatalytic activity in reduced $LaFeO_3$ films, Chem Commun, 53 (2017) 2499-2502.
[14] H. Han, D. Kim, K. Chu, J. Park, S.Y. Nam, S. Heo, C.H. Yang, H.M. Jang, Enhanced Switchable Ferroelectric Photovoltaic Effects in Hexagonal Ferrite Thin Films via Strain Engineering, ACS applied materials & interfaces, 10 (2018) 1846-1853.

[15] R. Jiménez, J. Ricote, I. Bretos, R.J. Jiménez Riobóo, F. Mompean, A. Ruiz, H. Xie, M. Lira-Cantú, M.L. Calzada, Stress-mediated solution deposition method to stabilize ferroelectric $BiFe_{1-x}Cr_xO_3$ perovskite thin films with narrow bandgaps, Journal of the European Ceramic Society, 41 (2021) 3404-3415.
[16] M. Zheng, H. Sun, K.W. Kwok, Mechanically controlled reversible photoluminescence response in all-inorganic flexible transparent ferroelectric/mica heterostructures, NPG Asia Materials, 11 (2019) 52.
[17] M. Zheng, X.-Y. Li, H. Ni, X.-M. Li, J. Gao, van der Waals epitaxy for highly tunable all-inorganic transparent flexible ferroelectric luminescent films, Journal of Materials Chemistry C, 7 (2019) 8310-8315.
[18] L. Su, X. Lu, L. Chen, Y. Wang, G. Yuan, J.M. Liu, Flexible, Fatigue-Free, and Large-Scale $Bi_{3.25}La_{0.75}Ti_3O_{12}$ Ferroelectric Memories, ACS applied materials & interfaces, 10 (2018) 21428-21433.
[19] C.H. Ma, J. Jiang, P.W. Shao, Q.X. Peng, C.W. Huang, P.C. Wu, J.T. Lee, Y.H. Lai, D.P. Tsai, J.M. Wu, S.C. Lo, W.W. Wu, Y.C. Zhou, P.W. Chiu, Y.H. Chu, Transparent Antiradiative Ferroelectric Heterostructure Based on Flexible Oxide Heteroepitaxy, ACS applied materials & interfaces, 10 (2018) 30574-30580.
[20] M. Zheng, H. Sun, M.K. Chan, K.W. Kwok, Reversible and nonvolatile tuning of photoluminescence response by electric field for reconfigurable luminescent memory devices, Nano Energy, 55 (2019) 22-28.
[21] M.N. Kamalasanan, S. Chandra, Structural and optical properties of sol-gel-processed $BaTiO_3$ ferroelectric thin films, Applied Physics Letters, 59 (1991) 3547.
[22] X.H. Wang, J.G. Li, H. Kamiyama, M. Katada, N. Ohashi, Y. Moriyoshi, T. Ishigaki, Pyrogenic Iron(III)-Doped TiO_2 Nanopowders Synthesized in RF Thermal Plasma: Phase Formation, Defect Structure, Band Gap, and Magnetic Properties, Journal of American Chemical Society, 127 (2005) 10982-10990.
[23] P. Singh, I. Choudhuri, H.M. Rai, V. Mishra, R. Kumar, B. Pathak, A. Sagdeo, P.R. Sagdeo, Fe doped $LaGaO_3$: good white light emitters, RSC Advances, 6 (2016) 100230-100238.
[24] T. Mizokawa, A. Fujinmori, Electronic structure and orbital ordering in perovskite-type 3*d* transition-metal oxides studied by Hartree-Fock band-structure calculations, Physical Review B, 54 (1996) 5368.
[25] S.A. Akhade, J.R. Kitchin, Effects of strain, d-band filling, and oxidation state on the bulk electronic structure of cubic 3*d* perovskites, The Journal of Chemical Physics, 135 (2011) 104702.

[26] R.F. Berger, C.J. Fennie, J.B. Neaton, Band gap and edge engineering via ferroic distortion and anisotropic strain: the case of $SrTiO_3$, Physical review letters, 107 (2011) 146804.
[27] N. Vonrüti, U. Aschauer, Epitaxial strain dependence of band gaps in perovskite oxynitrides compared to perovskite oxides, Physical Review Materials, 2 (2018) 105401.
[28] C.J. Xiao, Z.H. Chi, W.W. Zhang, F.Y. Li, S.M. Feng, C.Q. Jin, X.H. Wang, X.Y. Deng, L.T. Li, The phase transitions and ferroelectric behavior of dense nanocrystalline $BaTiO_3$ ceramics fabricated by pressure assisted sintering, Journal of Physics and Chemistry of Solids, 68 (2007) 311-314.
[29] I.s.B. Ouni, D. Chapron, H. Aroui, M.D. Fontana, Ca doping in $BaTiO_3$ crystal: Effect on the Raman spectra and vibrational modes, Journal of Applied physics, 121 (2017) 113102.
[30] M.S. Chen, Z.X. Shen, S.H. Tang, W.S. Shi, D.F. Cui, Z.H. Chen, Stress effect on Raman spectra of Ce-doped $BaTiO_3$ films, Journal of Physics: Condensed Matter, 12 (2000) 7013-7023.
[31] M.D. Scafetta, A.M. Cordi, J.M. Rondinelli, S.J. May, Band structure and optical transitions in $LaFeO_3$: theory and experiment, Journal of physics. Condensed matter : an Institute of Physics journal, 26 (2014) 505502.
[32] K.J. Choi, M. Biegalski, Y.L. Li, A. Sharan, J. Schubert, R. Uecker, P. Reiche, Y.B. Chen, X.Q. Pan, V. Gopalan, L.Q. Chen, D.G. Schlom, C.B. Eom, Enhancement of Ferroelectricity in Strained $BaTiO_3$ Thin Films, Science, 306 (2004) 1005-1009.
[33] K.T. Kang, H.I. Seo, O. Kwon, K. Lee, J.-S. Bae, M.-W. Chu, S.C. Chae, Y. Kim, W.S. Choi, Ferroelectricity in $SrTiO_3$ epitaxial thin films via Sr-vacancy-induced tetragonality, Applied Surface Science, 499 (2020) 143930.
[34] J. Belhadi, F. Ravaux, H. Bouyanfif, M. Jouiad, M. El Marssi, Quantification and mapping of elastic strains in ferroelectric $[BaZrO_3]_x/[BaTiO_3]_{(1-x)}$ superlattices, Applied Surface Science, 512 (2020) 145761.